Applied and Computational Mechanics 4 (2010) 251–262

Modelling of the mechanical behaviour of porcine carotid artery undergoing inflation-deflation test

J. Vychytil[a,*], F. Moravec[a], P. Kochová[a], J. Kuncová[b], J. Švíglerová[b]

[a] *Faculty of Applied Sciences, University of West Bohemia, Univerzitní 22, 306 14 Plzeň, Czech Republic*
[b] *Faculty of Medicine in Pilsen, Charles University in Prague, Lidická 1, 301 66 Plzeň, Czech Republic*

Received 17 September 2010; received in revised form 1 December 2010

Abstract

Samples of porcine carotid artery are examined using Tissue bath MAYFLOWER, Perfusion of tubular organs Version, Type 813/6. Pressure-diameter diagrams are obtained for fixed axial extension and volumetric flow rate. Finite element analysis of the experiment, performed using COMSOL software, indicates a negligible effect of given flow rate on the mechanical response of the tested sample. Also the effect of clamped ends is shown to be local only. Hence, static analysis in MATLAB software is performed considering the arterial segment as an incompressible hyperelastic axisymmetric tube. Residual stress at the load-free configuration is taken into account resulting in the overall stiffening of the model. Comparison of theoretical and experimental pressure-diameter curves results in the identification of material parameters using the least square method. In addition to classical hyperelastic models, such as the neo-Hookean and the Fung's exponential, two-scale model mimicking arrangement of soft tissue is considered.

Keywords: carotid artery, inflation-deflation test, modelling, hyperelasticity, parameters identification

1. Introduction

The arterial wall mechanics and its interaction with blood flow have been an object of extensive research during past decades. Many experiments have been performed to investigate the material properties of animal and human arteries, see e.g. [8, 12, 13]. Earlier works on this topic date back to the end of the 19th century, such as the work [27] proving mechanical response of arteries to be nonlinear with strain-hardening. The common assumption of incompressibility is confirmed in [5] observing volume change to be very small even for deformations greater than those *in vivo*. The anisotropy of the arterial wall is an evident fact due to the enormous complexity of its microstructure. However, experiments performed in [24] suggest that arterial segments can be considered as cylindrically orthotropic tubes for modelling purposes. According to [15, 22] material constants are found to be of the order ~ 1 MPa for elastic modulus and its fraction of approximately 1/10 for loss modulus. However, mechanical properties depend on many factors, such as age and volume fraction of constituents, see e.g. [1, 2].

Together with experiments, numerical modelling plays an important role in understanding arterial mechanics. Since the blood flow through an artery represents a complex problem of fluid-solid interaction in the framework of continuum mechanics, simplifications concerning both arterial wall and flow are applied. In [29], for instance, the bypass model is proposed considering arterial walls as rigid and the blood flow as incompressible Newtonian. More often,

*Corresponding author. Tel.: +420 377 632 380, e-mail: vychytil@kme.zcu.cz.

arterial walls are considered as hyperelastic [28] or linearly viscoelastic [4]. Such assumption is supported by a biaxial tension test performed with porcine coronary artery tissue in [21]. Although the anisotropy of the tissue is demonstrated, isotropic models are sufficient to describe *in vivo* conditions according to authors. On the other hand, isotropic hyperelastic (viscoelastic) models cannot be capable of describing all aspects of the mechanical response of the arterial wall resulting from its complex microstructure and from the fact that artery is a living tissue. According to [26], relevant features that should not be omitted in the modelling of arteries include anisotropy, residual stresses and remodeling. Therefore, the latest works deal with these effects and possible modelling approaches.

An anisotropy of the arterial wall can be described using the notion of fiber-reinforced materials [18]. This approach is applied in [14, 19] to propose a hyperelastic model of arterial wall. The fibrous nature of the arterial wall is included in the formula of strain-energy function via two unit vectors representing the orientations of collagenous fibers. Extension for the case of viscoelastic response is done in [20]. A different approach is proposed in [31] by defining the eight-chain orthotropic unit element that represents the microstructure. Employing the assumption of affine deformations at the micro-scale, an orthotropic hyperelastic material model of the arterial wall is obtained.

It is known fact that unloaded arteries are not stress-free due to the certain growth mechanisms of the different layers. Also, they are subjected to axial prestretch *in vivo*, see e.g. [7, 9, 19]. Theoretical framework for dealing with residual stress in arteries is provided in [19]. It consists in introducing three configurations: reference (stress-free), unloaded and current. The simplification of geometry of the arterial ring leads to a description of the residual stress with a single parameter. A similar approach is used in [9] to propose a finite element (FE) model of the carotid segment. Here, residual stress causes the resulting stress field to be much more uniform. In [23], the model of prestrained cytoskeleton is embedded into a macroscopic model of arterial wall using the method of homogenization. Although the model of arterial ring opens, which is in agreement with observations, author admits that it does not reflect a realistic situation. A similar approach of including prestress in the material model (using the model of prestressed cytoskeleton and the notion of representative volume element) is described in [30].

Finally, recent works on numerical modelling of arterial walls deal also with the so-called remodeling, i.e. change of either geometry or mechanical properties in order to adapt to applied load [26]. In [16], for instance, the reorientation of collagen fibers within arterial wall is modelled upon the assumption of their alignment with the directions of principal stresses.

The aim of this work is to investigate the mechanical response of the porcine carotid artery experimentally and to propose a suitable model representing the artery under experimental conditions. The paper is organized as follows. Section 2 describes an experiment which consists in loading the arterial segment with inner pressure under constant flow rate and axial prestretch. Pressure-diameter diagrams for both inflation (loading) and deflation (unloading) parts are provided. In section 3, preliminary estimates and an FE analysis of the artery under experimental conditions is performed. The simplified geometry of axisymmetric tube is considered using the hyperelastic material models of the neo-Hookean and the Fung's type, the fluid is considered to be incompressible Newtonian. Results indicate a negligible effect of flow rate substantiating the static analysis performed in MATLAB software in section 4. Here the arterial segment is represented as a hyperelastic tube loaded with inner pressure considering residual stress at the load-free configuration. Apart of the neo-Hookean and the Fung's model, the two-scale hyperelastic model introduced in [17] is employed. A comparison with experiment is provided using the least square method which leads to the identification of material parameters.

2. Experimental investigation of the artery

2.1. Experimental setting

The porcine carotid artery is obtained from domestic pig. The animal is firstly anesthetized and after dissection of the carotid artery, it is euthanized by KCl injection. The sample is prepared by cutting the segment of the artery with the length L and clamped into a measurement device (Tissue bath MAYFLOWER, Perfusion of tubular organs version, type 813/6, Hugo Sachs Electronik, Germany), see fig. 1. The sample is prestretched axially within the device to mimic *in vivo* conditions with $\lambda_z = 1.5$ so that its current length is $l = \lambda_z L$. This value is chosen according to the studies [11] and [25] where the value of 1.4 is used for common arteries in rabbits and 1.5 for porcine carotid arteries, respectively. In [19] the values between 1.1 and 1.9 are chosen depending on the kind of artery. The sample is embedded in the tissue bath and perfused intraluminarly with a constant flow rate $Q = 2$ ml/min. The Tyrode's solution with the temperature of $36\,^{\circ}$C is used. The measurement device provides for setting the outlet pressure, denoted with p_2 in fig. 1. At the same time, the outer diameter of the arterial segment is determined as follows. For each value of p_2, the middle segment of the artery of the length $l_m = 21$ mm (corresponding to $L_m = 14$ mm at the load-free state) is captured using stereomicroscope (Olympus SZ60) and camera (Olympus E440). Three values of diameter are measured from each photograph in the middle and both ends of measured segment. The resultant diameter is calculated as the arithmetic mean, i.e. $d = (d_1 + d_2 + d_3)/3$.

At first, the preconditioning of 4 cycles from 0 up to 200 mm Hg is performed to ensure unambiguous mechanical response. After that, the sample is loaded from 0 up to 200 mm Hg using the step of 10 mm Hg and then unloaded to 0 mm Hg using the same step. In fact, it is a

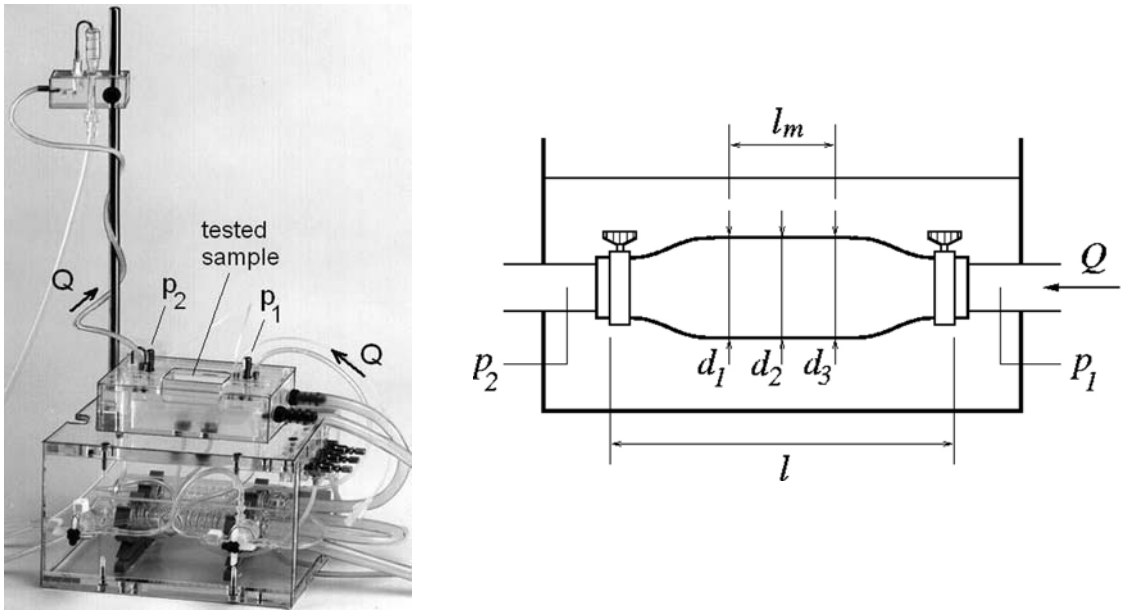

Fig. 1. The measurement device (left, taken with modifications from [32]) and the detailed scheme of clamped sample (right). The Tyrode's solution is pumped through the tested sample with constant flow rate of Q. The outlet pressure, p_2, is controlled by the device mounted on the stool. The inlet pressure is denoted with p_1. The arterial sample is clamped to the ends of two rigid pipes and prestretched axially to the current length of l. Outer diameters, d_1, d_2 and d_3 are measured in the middle segment of the length l_m

quasi-static process as setting each loading step and taking a photograph is done manually. The time of whole cycle is approximately $t \approx 6$ min providing $t_{step} \approx 9$ s for each step.

2.2. Results

The pressure-diameter diagram for whole inflation-deflation cycle is depicted in fig. 2. Both inflation and deflation parts exhibit the strain hardening as it is characteristic for soft living tissues, the hysteresis corresponds to the viscoelastic behaviour of the arterial wall. For convenience, the units of pressure are converted as 1 mm Hg $= 133.322$ Pa.

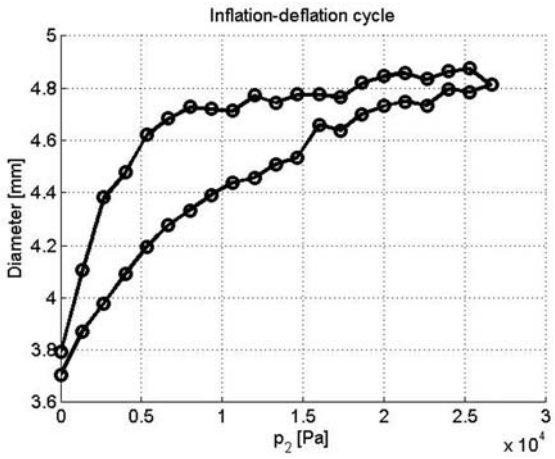

Fig. 2. The pressure-diameter diagram of the porcine carotid artery. The lower curve corresponds to inflation, the upper curve to deflation part of the cycle, respectively

3. Preliminary estimates and FE analysis

3.1. Fluid pressure, clamping effect

The Tyrode's solution is considered as an incompressible Newtonian fluid with the same characteristics as water, i.e. $\eta = 0.001$ Pa.s and $\rho = 1\,000\ \mathrm{kg} \cdot \mathrm{m}^{-3}$ (viscosity and mass density). The flow obeys the incompressible Navier-Stokes equations.

Considering the arterial segment as a cylindrical tube, the pressure corresponding to the laminar flow exhibits a linear decrease,

$$p(z) = \frac{p_1 - p_2}{l} z + p_2 \,, \tag{1}$$

see e.g. [3]. Here, z denotes the coordinate aligned with the longitudinal axis of the tube, $z = 0$ and $z = l$ refer to the outlet and the inlet region, respectively. The pressure difference can be estimated using the Poiseuille's formula for a laminar flow,

$$Q = \frac{\pi r_{in}^4}{8} \frac{p_1 - p_2}{\mu l} \,, \tag{2}$$

where r_{in} denotes the inner radius of the tube. In our case, the estimate of $(p_1 - p_2) \sim 1$ Pa is obtained. Comparing to the applied load (each step $\sim 10^2$ Pa), the pressure corresponding to the flow is negligible and thus the arterial segment can be considered as statically loaded with the inner pressure $\Delta P \approx p_2$.

Although the arterial segment can be represented with a cylindrical tube at the unloaded configuration, its shape at the current configuration is in fact more complex. However, for loading consisting of the inner pressure and the longitudinal stretch, the representation with the cylindrical tube is appropriate for the middle part, far enough from clamped ends.

3.2. FE analysis

To confirm the assumptions resulting from the preliminary estimates, the FE analysis is performed. The arterial segment is represented as a cylindrical tube at the reference configuration and residual stresses are not taken into account. Considering the axial symmetry, the fluid occupies the rectangle $[0, R_{in}] \times [0, L]$ and the solid occupies the rectangle $[R_{in}, R_{out}] \times [0, L]$ at the reference configuration. Here, $R_{in} = 1.07$ mm, $R_{out} = 2.38$ mm and $L = 14$ mm.

The solid part (i.e. the arterial wall) is considered as a hyperelastic incompressible material. The neo-Hookean and the Fung's energy functions are employed, their expressions as well as particular choice of material constants are detailed in section 4. The fluid part is considered as an incompressible Newtonian fluid, as it is mentioned in previous section.

Boundary conditions of the model are defined as follows. For the fluid, the constant inlet flow rate of $Q = 2$ ml/min and the outlet pressure p_2 are prescribed. The solid part is stretched along the z-axis at first with $\lambda_z = 1.5$ and then the left ($Z = 0$) and the right ($Z = L$) faces are fixed to represent clamping of the sample.

The results are depicted in figs. 3 to 6. In fig. 3, the distribution of the Von Mises stress at the current configuration of the solid part is depicted. The profile of the tube at the current

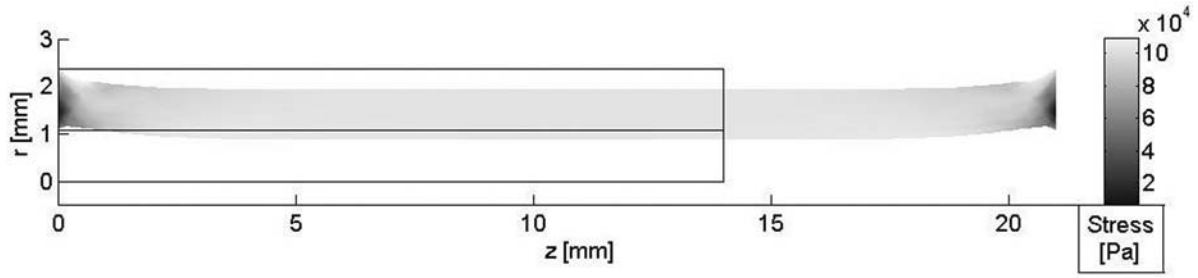

Fig. 3. Deformation and Von Mises stress distribution in the arterial wall involved by the stretch ratio of $\lambda_z = 1.5$ and the flow rate $Q = 2$ ml/min. Reference geometry is also indicated

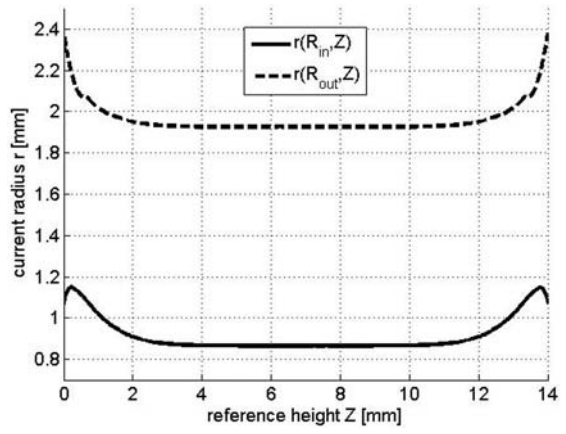

Fig. 4. Pipe profile at the current configuration for outlet pressure $p_2 = 0$ Pa

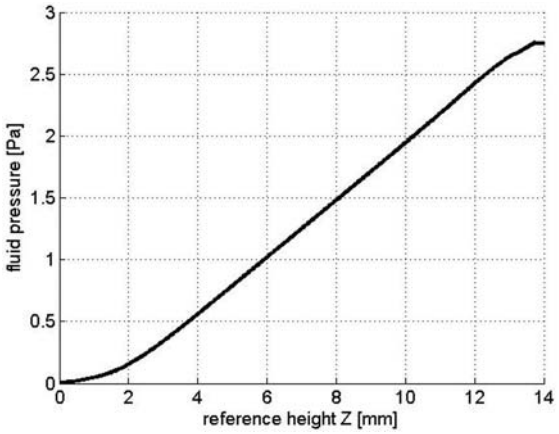

Fig. 5. Dependence of the fluid pressure on the height Z for outlet pressure $p_2 = 0$ Pa

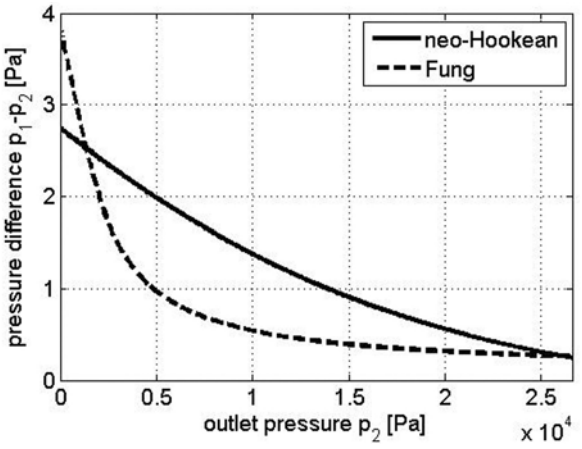

Fig. 6. Dependence of the difference between the inlet and outlet pressure on the outlet pressure with constant inner flow $Q = 2$ ml/min

configuration is also depicted in fig. 4. The distribution of the fluid pressure along the longitudinal axis is plotted in fig. 5. The dependence is nearly linear according to (1) except for the regions influenced by clamped ends. The pressure difference between the inlet and outlet region is small compared to stresses within the arterial wall and it even decreases with increasing outlet pressure, see fig. 6. Clearly, the assumptions resulting from preliminary estimations are confirmed. The clamping effect is only local and the pressure corresponding to the flow of the Tyrode's solution is negligible.

4. Static analysis

4.1. Basic relations

Description of deformations of the arterial wall follows the approach presented in [19]. To take into account the residual stresses, three configurations are introduced, see fig. 7. The reference configuration, Ω_0, corresponds to cut arterial segment that is supposed to be stress-free. The position of any material point is described using the cylindrical coordinate system $\{R, \Theta, Z\}$, where $R \in [R_{in}, R_{out}]$, $\Theta \in [0, 2\pi - \alpha]$ and $Z \in [0, L]$. Here, α denotes the opening angle. At the current configuration, the spatial coordinates are denoted with $\{r, \theta, z\}$, where $r \in [r_{in}, r_{out}]$, $\theta \in [0, 2\pi]$ and $z \in [0, l]$.

No shear occurs at the current state, hence the deformation gradient at the cylindrical coordinates takes the form

$$\mathbf{F} = \begin{pmatrix} r'(R) & 0 & 0 \\ 0 & \frac{hr}{R} & 0 \\ 0 & 0 & \lambda_z \end{pmatrix}. \tag{3}$$

Here, h is a constant parameter related to the opening angle and λ_z is a constant axial stretch,

$$h = \frac{2\pi}{2\pi - \alpha}, \quad \lambda_z = \frac{l}{L}. \tag{4}$$

The arterial wall is assumed to be incompressible providing the expression for current radius as

$$r(R) = \sqrt{\frac{R^2}{h\lambda_z} + C}. \tag{5}$$

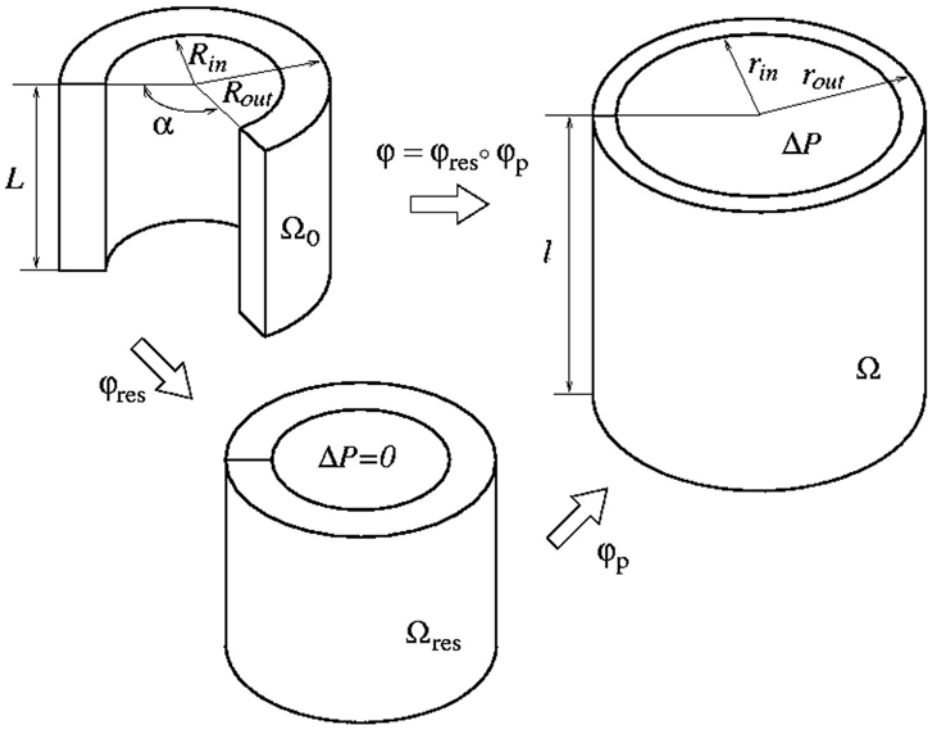

Fig. 7. An arterial segment at the stress-free reference configuration Ω_0, the load-free configuration Ω_{res} and the current configuration Ω. Redrawn with modifications from [19]

Here, C is to be determined from the boundary conditions. Applying the momentum balance,

$$\frac{\partial \sigma_{rr}}{\partial r} + \frac{1}{r}\left(\sigma_{rr} - \sigma_{\theta\theta}\right) = 0\,, \tag{6}$$

the constitutive equation of hyperelasticity,

$$\boldsymbol{\sigma} = \frac{\partial \hat{W}}{\partial \mathbf{F}}\mathbf{F}^T - p\mathbf{I}\,, \tag{7}$$

and the boundary conditions,

$$\sigma_{rr}(r_{in}) = -\Delta P,\,, \quad \sigma_{rr}(r_{out}) = 0\,, \tag{8}$$

we obtain the relationship between ΔP and C,

$$\Delta P = \int_{R_{in}}^{R_{out}} \frac{r'}{r}\left(\frac{r}{R}\hat{W}_2 - r'\hat{W}_1\right)\mathrm{d}R\,. \tag{9}$$

Here, $\boldsymbol{\sigma}$ is the Cauchy stress tensor, p is the hydrostatic pressure, ΔP is the pressure applied to the inner face of the tube and $\hat{W}_i$ denotes the partial derivative of $\hat{W}$ with respect to the corresponding diagonal component of the deformation gradient,

$$\hat{W}_i = \frac{\partial \hat{W}}{\partial \lambda_i}\,, \quad \lambda_i = F_{ii}\,. \tag{10}$$

4.2. Material models

Three material models defined by various formulas of strain-energy functions are employed. The isotropic neo-Hookean and the anisotropic Fung's material model are defined as

$$\begin{aligned} \hat{W}_{NH} &= \frac{\mu}{2}\left(\operatorname{tr}\hat{\mathbf{C}} - 3\right) , \\ \hat{W}_{Fung} &= \frac{c}{2}\left[\exp(q) - 1\right] , \end{aligned} \tag{11}$$

where $\hat{\mathbf{C}} = (\det \mathbf{C})^{-1/3}\mathbf{C}$, $\mathbf{C} = \mathbf{F}^T\mathbf{F}$, μ and c are material parameters. The function q in the Fung's model is defined as

$$\begin{aligned} q = b_1\hat{E}_{\theta\theta}^2 + b_2\hat{E}_{zz}^2 + b_3\hat{E}_{rr}^2 + 2b_4\hat{E}_{\theta\theta}\hat{E}_{zz} + 2b_5\hat{E}_{zz}\hat{E}_{rr} + \\ 2b_6\hat{E}_{rr}\hat{E}_{\theta\theta} + b_7\hat{E}_{\theta z}^2 + b_8\hat{E}_{rz}^2 + b_9\hat{E}_{r\theta}^2 . \end{aligned} \tag{12}$$

Here, $\hat{E}_{ij}$ are the components of the Green-Lagrange strain tensor referred to cylindrical coordinates, b_i's are non-dimensional material parameters.

Also, the so-called "balls and springs" (BS) model introduced in [17] is employed. It is a two-scale orthotropic hyperelastic model motivated by the arrangement of the microstructure of soft tissues. Its mechanical response can be described by an approximative analytical formula of strain-energy function,

$$W_{bs} = W_s + W_m , \tag{13}$$

where

$$W_s = \frac{1}{2}\sum_{\substack{i=1 \\ i\neq j\neq k}}^{3} K_i \frac{k_i}{1+k_i} l_{ij} l_{ik} \left[(F_{ii} - 1) + \gamma_i P_i\right]^2 , \tag{14}$$

and

$$W_m = \frac{K_1K_2K_3(1+k_1)(1+k_2)(1+k_3)\left[1 - F_{11}^{eff}F_{22}^{eff}F_{33}^{eff}\right]^2}{\sum_{i=1,i\neq j\neq k}^{3} 2K_jK_k(1+k_j)(1+k_k)\frac{l_{ji}l_{ki}}{\gamma_i^2}\left(F_{jj}^{eff}F_{kk}^{eff}\right)^2} . \tag{15}$$

Here, K_i's, k_i's, l_{ij}'s and γ_i's are material parameters related to the microstructure (stiffness of matrix and cells, geometrical anisotropy, relative sizes of cells), see [17, 30] for details. The effective stretches are defined as

$$F_{ii}^{eff} = \frac{F_{ii} - 1}{\gamma_i(1+k_i)} + 1 . \tag{16}$$

In general, this orthotropic model contains 11 material parameters. However, this number is reduced for the case of transverse isotropy (7 material parameters) or isotropy (3 material parameters).

4.3. Influence of residual stresses

To obtain pressure-diameter curves, equations derived in this section are implemented in MATLAB software. For a given pressure ΔP, the unknown constant C is determined from (9) using the Newton-Raphson iteration scheme. The diameter is then calculated using (5) as

$$d = 2r(R_{out}) . \tag{17}$$

The influence of residual stresses on the mechanical response is studied by controlling the parameter α (the opening angle, see fig. 7). If $\alpha = 0$, no residual stress is involved, i.e. the load-free configuration is also stress-free. Increasing value of α then accounts for increasing residual stress. The pressure-diameter curves for various values of α are plotted in fig. 8 for the neo-Hookean and the Fung's model. The geometry of the segment is characterized with $R_{in} = 1.07$ mm, $R_{out} = 2.38$ mm, and the axial stretch is $\lambda_z = 1.5$. The material parameters are chosen as those resulting from identification in the following section. For both material models, the tube stiffens with increasing residual stress, i.e. certain value of inner pressure ΔP causes smaller deformation of diameter d when opening angle α increases.

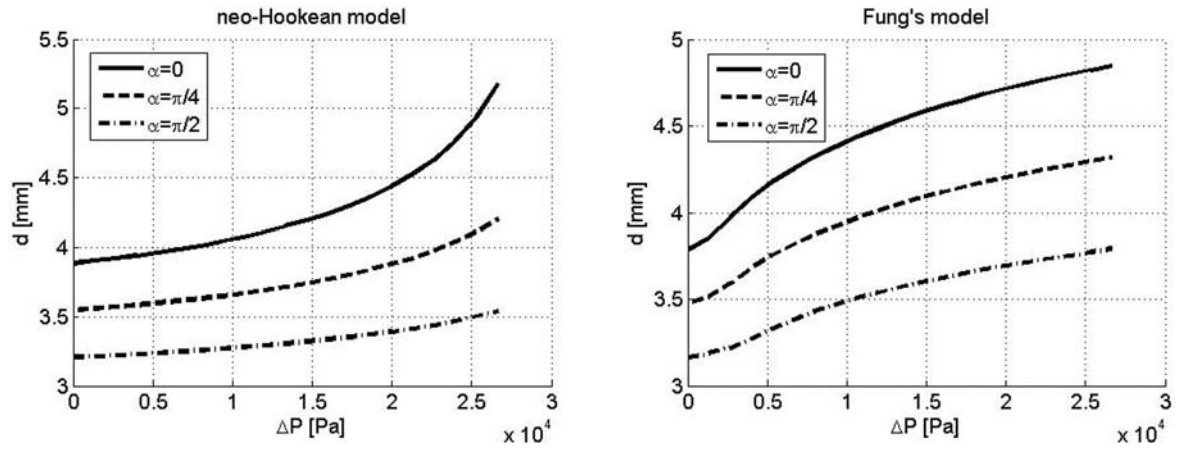

Fig. 8. Influence of the residual stress on the mechanical response of the arterial segment. The neo-Hookean (left) and the Fung's model (right) are employed with different values of opening angle α. Curves describe the dependence of outer diameter d on the applied inner pressure ΔP

4.4. Comparison with experiment

Theoretical pressure-diameter curves are compared with the inflation part of the experimental cycle depicted in fig. 2. The geometry of the model is obtained from measurements of the cut arterial segment. It is $R_{in} = 1.58$ mm, $R_{out} = 2.77$ mm, opening angle $\alpha = 0.41\,\pi$ and the axial stretch is $\lambda_z = 1.5$. A comparison with experimental data is provided using the least

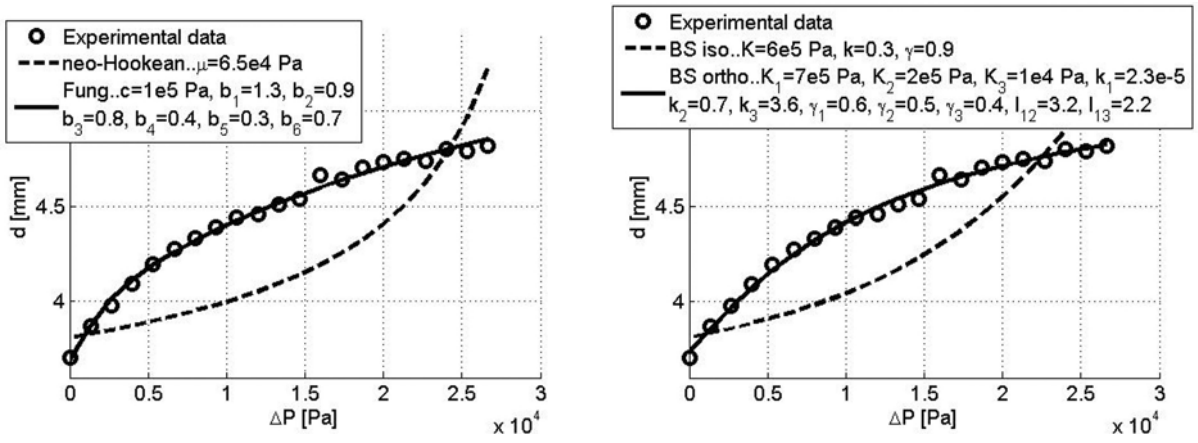

Fig. 9. Comparison of theoretical pressure-diameter curves with experimental data involving the inflation part of the cycle. The neo-Hookean and the Fung's model are depicted on the left, the BS approximative model (both orthotropic and isotropic) on the right figure

square method which leads to the identification of material parameters. Results for the neo-Hookean, the Fung's and the BS model are depicted in fig. 9. Approximate values of material parameters of each model resulting from identification are listed in boxes.

The neo-Hookean as well as the isotropic restriction of the BS model exhibit opposite pattern compared to the experiment (strain-softening instead of strain-hardening). Therefore, theoretical curves of these models do not fit experimental data. The Fung's exponential and the BS orthotropic models, on the other hand, exhibit a good agreement with experiment proving their applicability for the modelling of arterial walls.

5. Conclusion

The mechanical response of the porcine carotid artery exhibits typical patterns of soft tissues. After preconditioning, both strain-hardening and hysteresis are observed during inflation and deflation phases. In the experiment, the sample is prestretched axially to mimic *in vivo* conditions.

The preliminary estimates and the following FE analysis indicate that the arterial segment under the experimental conditions can be represented as a cylindrical tube loaded statically with the inner pressure and the axial stretch. The analysis is performed considering the load-free configuration to be stress-free for simplicity. However, the same conclusions can be expected when the residual stress is taken into account as its contribution to the mechanical response is the overall stiffening.

Adopting these assumptions, the static analysis is performed considering the arterial segment as an incompressible hyperelastic tube. Here, both axial prestretch and residual stress are taken into account. Influence of the residual stress consists in the stiffening of the model, i.e. it can be understood as a subsidiary mechanism of arteries to bear loads caused by pulsatile blood flow and to reduce inadequate deformations *in vivo*. However, residual stress is taken into account via a single parameter in this model considering the open arterial segment as stress-free. In real arteries, residual stress is a more complex problem resulting from certain growth mechanisms of the different layers.

Comparison of theoretical pressure-diameter curves with experimental data is provided for the neo-Hookean, the Fung's and the so-called "balls and springs" (BS) material model. Both the Fung's and the BS models provide a good agreement with experiment due to their anisotropy and a large number of material constants (7 and 11, respectively). The neo-Hookean and the isotropic restriction of the BS model, on the other hand, exhibit an opposite pattern (strain-softening) in the mechanical response when compared to the experiment. Therefore, these models do not seem to be suitable for the modelling of arterial walls. Values of the material parameters found for the Fung's model seem to be reasonable although in [6] slightly different values for a rabbit carotid artery were obtained. Namely, $c \sim 10^4$ Pa, b_1 and $b_2 \sim 10^{-1}$, $b_3 \sim 10^{-3}$ and b_4 to $b_6 \sim 10^{-2}$. Apart of different tissue, material parameters are obtained upon an assumption of a stress-free state at the load-free configuration which may also lead to different results. Material constant found for the neo-Hookean model corresponds to the Young's modulus of $\approx 2 \times 10^5$ Pa. It does not correspond to the Young's modulus of the examined tissue since the mechanical response of the neo-Hookean model differs significantly from the experimental observation. However, the same order of value for dynamic elastic moduli are obtained in [15, 10] for carotid human arteries ($0.49 - 6.08 \times 10^5$ Pa) and arteries of dogs ($\sim 10^5$ Pa).

Concerning the BS model, the approximative analytical formula of the strain energy function is employed in this work for simplicity. Although it exhibits a good agreement with exper-

iment, the approximative formula is in fact not accurate for the values of material parameters obtained in the identification. In other words, it does not represent the material with its microstructure as proposed in [17]. Rather, it may be understood as a phenomenological model.

Aims for the future are to consider accurate formula of the BS model capturing the microstructure and including prestress with the possible application on the study of activation and contraction of living tissue. To consider various experimental and modelling conditions such as the variation of flow rate, dynamic and cyclic loading and to describe hysteresis in the mechanical response as well as time dependent behaviour, viscoelastic models must be employed. Possible approach for creating such models, for instance, is the notion of internal variables. Challenging topic is also the degradation of tissue at the microlevel caused by the collagenase and elastase treatment. Modelling of the mechanical response of the degraded tissue using the BS model is of further interest.

Acknowledgements

The work has been supported by the grant project GAČR 106/09/0734 and by the research project MSM 4977751303.

References

[1] Apter, J. T., Rabinowitz, M., Cummings, D. H., Correlation of visco-elastic properties of large arteries with microscopic structure, Circulation Research 19 (1966) 104–121.

[2] Bader, H., Dependence of wall stress in the human thoracic aorta on age and pressure, Circulation Research 20 (1967) 354–361.

[3] Brdička, M., Samek, L., Sopko, B., Mechanika kontinua, 2nd Edition, Academia, Praha, 2000.

[4] Čanić, S., Hartley, C. J., Rosenstrauch, D., Tambača, J., Guidoboni, G., Mikelić, A., Blood flow in compliant arteries: An effective viscoelastic reduced model, numerics, and experimental validation, Annals of Biomedical Engineering 34 (4) (2006) 575–592.

[5] Carew, T. E., Vaishnav, R. N., Patel, D. J., Compressibility of the arterial wall, Circulation Research 23 (1968) 61–68.

[6] Chuong, C. J., Fung, Y. C., Three-dimensional stress distribution in arteries, Journal of Biomechanical Engineering 105 (1983) 268–274.

[7] Chuong, C. J., Fung, Y. C., On residual stresses in arteries, Journal of Biomechanical Engineering 108 (1986) 189–192.

[8] Cox, R. H., Passive mechanics and connective tissue composition of canine arteries, American Journal of Physiology 234 (1978) 533–541.

[9] Delfino, A., Stergiopulos, N., Moore, J. E., Meister, J. J., Residual strain effects on the stress field in a thick wall finite element model of the human carotid bifurcation, Journal of Biomechanics 30 (8) (1997) 777–786.

[10] Either, C. R., Simmons, C. A., Introductory biomechanics. From cells to organisms, Cambridge university press, Cambridge, 2008.

[11] Fonck, E., Prod'hom, G., Roy, S., Augsburger, L., Rüfenacht, D. A., Stergiopulos, N., Effect of elastin degradation on carotid wall mechanics as assessed by a constituent-based biomechanical model, American Journal of Physiology – Heart and Circulatory Physiology 292 (2007) H2754–H2763.

[12] Fridez, P., Makino, A., Miyazaki, H., Meister, J. J., Hayashi, K., Stergiopulos, N., Short-term biomechanical adaptation of the rat carotid to acute hypertension: Contribution of smooth muscle, Annals of Biomedical Engineering 29 (1) (2001) 26–34.

[13] Fridez, P., Zulliger, M., Bobard, F., Montorzi, G., Miyazaki, H., Hayashi, K., Stergiopulos, N., Geometrical, functional, and histomorphometric adaptation of rat carotid artery in induced hypertension, Journal of Biomechanics 36 (2003) 671–680.

[14] Gasser, T. C., Ogden, R. W., Holzapfel, G. A., Hyperelastic modelling of arterial layers with distributed collagen fibre orientation, Journal of the Royal Society Interface 3 (2006) 15–35.

[15] Gow, B. S., Taylor, M. G., Measurement of viscoelastic properties of arteries in the living dog, Circulation Research 23 (1968) 111–122.

[16] Hariton, I., de Botton, G., Gasser, T. C., Holzapfel, G. A., Stress-driven collagen fiber remodeling in arterial walls, Biomechanics and Modeling in Mechanobiology 6 (2007) 163–175.

[17] Holeček, M., Moravec, F., Hyperelastic model of a material which microstructure is formed of "balls and springs", International Journal of Solids and Structures 43 (2006) 7 393–7 406.

[18] Holzapfel, G. A., Nonlinear solid mechanics, Wiley, Chichester, 2000.

[19] Holzapfel, G. A., Gasser, T. C., Ogden, R. W., A new constitutive framework for arterial wall mechanics and a comparative study of material models, Journal of Elasticity 61 (2000) 1–48.

[20] Holzapfel, G. A., Gasser, T. C., Stadler, M., A structural model for the viscoelastic behavior of arterial walls: Continuum formulation and finite element analysis, European Journal of Mechanics A/Solids 21 (2002) 441–463.

[21] Lally, C., Reid, A. J., Prendergast, P. J., Elastic behavior of porcine coronary artery tissue under uniaxial and equibiaxial tension, Annals of Biomedical Engineering 32 (10) (2004) 1 355–1 364.

[22] Learoyd, B. M., Taylor, M. G., Alterations with age in the viscoelastic properties of human arterial walls, Circulation Research 18 (1966) 278–292.

[23] Lukeš, V., Two-scale computational modelling of soft biological tissues, Ph.D. thesis, University of West Bohemia in Pilsen, Pilsen, 2007.

[24] Patel, D. J., Fry, D. L., The elastic symmetry of arterial segments in dogs, Circulation Research 24 (1969) 1–8.

[25] Perrée, J., van Leeuwen, T. G., Kerindongo, R., Spaan, J. A. E., VanBavel, E., Function and structure of pressurized and perfused porcine carotid arteries, Effects of in vitro balloon angioplasty, American Journal of Pathology 163 (2003) 1 743–1 750.

[26] Rodríguez, J., Goicolea, J. M., García, J. C., Gabaldón, F., Finite element models for mechanical simulation of coronary arteries, Proceedings of the 2nd International Workshop on Functional Modeling of the Heart, Lyon, Springer, Lecture Notes in Computer Science 2674, 2003, pp. 295–305.

[27] Roy, C. S., The elastic properties of the arterial wall, The Journal of Physiology 3 (1880) 125–159.

[28] Valencia, A., Solis, F., Blood flow dynamics and arterial wall interaction in a saccular aneurysm model of the basilar artery, Computers and Structures 84 (2006) 1 326–1 337.

[29] Vimmr, J., Jonášová, A., Analysis of blood flow through three-dimensional bypass model, Applied and Computational Mechanics 1 (2) (2007) 693–702.

[30] Vychytil, J., Holeček, M., Two-scale hyperelastic model of a material with prestress at cellular level, Applied and Computational Mechanics 2 (1) (2008) 167–176.

[31] Zhang, Y., Dunn, M. L., Drexler, E. S., McCowan, C. N., Slifka, A. J., Ivy, D. D., Shandas, R., A microstructural hyperelastic model of pulmonary arteries under normo- and hypertensive conditions, Annals of Biomedical Engineering 33 (8) (2005) 1 042–1 052.

[32] Instruction manual: Tissue bath MAYFLOWER. Version: Perfusion of tubular organs Type 813/6. Hugo Sachs Electronik – Harvard apparatus GmbH, Germany. http://www.hugo-sachs.de